

NEAR-INFRARED SPECTROSCOPY OF SDSS J0303-0019:
A LOW LUMINOSITY, HIGH EDDINGTON RATIO QUASAR AT $Z \sim 6$

J. D. KURK¹, F. WALTER¹, X. FAN^{2,3}, L. JIANG², S. JESTER¹, H.-W. RIX¹, D. A. RIECHERS^{4,5}

Accepted by ApJ on July 1, 2009

ABSTRACT

We present sensitive near-infrared VLT ISAAC spectroscopic observations of the $z = 6.08$ quasar SDSS J030331.40–001912.9. This QSO is more than a magnitude fainter than other QSOs at $z \sim 6$ for which NIR spectroscopy has been obtained to date and is therefore presumably more representative of the QSO population at the end of Cosmic Reionization. Combining rest-frame UV continuum luminosity with the width measurements of the Mg II and C IV lines, we derive a black hole mass of $2_{-0.5}^{+1.0} \times 10^8 M_{\odot}$, the lowest mass observed for $z \sim 6$ QSOs to date, and derive an Eddington ratio of $1.6_{-0.6}^{+0.4}$, amongst the highest value derived for QSOs at any redshift. The Spitzer 24 μm non-detection of this QSO does not leave space for a significant hot dust component in its optical/near-infrared SED, in common with one other faint QSO at $z = 6$, but in contrast to more than twenty more $z = 6$ QSOs and all known lower redshift QSOs with sufficiently deep multi-wavelength photometry. We conclude that we have found evidence for differences in the intrinsic properties of at least one $z \sim 6$ QSO as compared to the lower-redshift population.

Subject headings: Galaxies: high-redshift — early Universe — quasars: emission lines — quasars: individual: SDSS J030331.40-001912.9

1. INTRODUCTION

The radiation from luminous quasi stellar objects (QSOs) can currently be studied up to redshift 6.5 and thus allows one to probe, over much of the Universe's age, the properties of their central black holes (BHs, e.g., Willott et al. 2003), their broad line region (BLR, e.g., Freudling et al. 2003), and the ionization state of intergalactic gas (e.g., Fan et al. 2006b). The most distant QSOs are of importance for both the study of galaxy evolution and large-scale structure. Among the most surprising discoveries in this field are the detection of BH masses $> 10^9 M_{\odot}$ (e.g., Barth et al. 2003; Willott et al. 2003) and the apparent constancy of the observed QSO BLR properties with redshift, even up to $z = 6.4$ (e.g., Pentericci et al. 2002), corresponding to an age of 870 Myr. E.g., the Fe II/Mg II (Freudling et al. 2003; Maiolino et al. 2003; Iwamuro et al. 2004; Kurk et al. 2007, hereafter K07) and N V/C IV (Jiang et al. 2007) emission line ratios observed in the BLR of $z > 6$ QSOs are as high as that observed in low-redshift objects. Thus, near-solar metallicity in the centers of some of the earliest systems and accretion of $> 10^9$ solar masses in a central BH can be attained in less than 1 Gyr. One caveat, however, has to be taken into account: until now only the most luminous objects at $z \sim 6$ have been studied. These objects may experience faster evolution than less luminous objects and therefore resemble low to intermediate redshift QSOs already at $z \sim 6$. Secondly, the relationships established using low-luminosity AGN (at low redshift) may not be valid for objects at the upper end of the luminosity distribution. As an example, the determination of the BH mass in active galaxies was cali-

brated with reverberation mapping observations of AGN that are one to two orders of magnitude fainter than the $z \sim 6$ QSOs observed until now (Kaspi et al. 2000). It is therefore important to extend $z \gtrsim 6$ studies to lower-luminosity objects. Here we present the first observations of a QSO at $z > 6$ with luminosity lower than $L_{\text{bol}} = 10^{47}$ erg s⁻¹: the QSO SDSS J030331.40-001912.9 (hereafter J0303-0019). This QSO was detected in the Sloan Digital Sky Survey (SDSS) Deep Stripe with a magnitude of $z_{\text{AB}} = 20.9$. Its discovery spectrum shows a very strong and narrow Ly α emission line at $z = 6.070$ (Jiang et al. 2008). As this line falls in the z -band, the actual continuum luminosity is low, $m_{1450} = 21.3$, 1.5 magnitudes fainter than the mean of the $z \sim 6$ QSO samples studied in K07 and Jiang et al. (2007). In addition, this is one of the two out of about twenty $z \sim 6$ QSOs that are not detected at 24 μm with MIPS/Spitzer, implying a rest frame 3.5 $\mu\text{m}/4400\text{\AA}$ ratio far lower than for any other known QSO (Jiang et al. 2006, L. Jiang et al. in prep.).

2. OBSERVATIONS AND REDUCTION

2.1. Near-infrared spectroscopy

NIR spectroscopy of J0303-0019 in the Y and K bands was obtained in service mode on December 24 and November 26 and 28, 2007, respectively, with ISAAC (Moorwood et al. 1998) at VLT UT1. We used the short wavelength arm, equipped with a 1024 \times 1024 Hawaii Rockwell array which has a pixel scale of 0.147". The 1" slit results in a spectral resolution of 550 and 450 for the Y and K bands, respectively. Observations were carried out in a standard ABBA offset pattern, with additional dithering to reduce the influence of bad pixels. Individual exposures were 148s, repeated 16 times per observing block. Nine such blocks were obtained in K band, for a total exposure time of ~ 5.9 hr, and two in Y band, for a total time of ~ 1.3 hr. The data were reduced using ESO's ISAAC pipeline software, which does flat fielding, back-

¹ MPIA, Königstuhl 17, 69117, Heidelberg, Germany
² Steward Observatory, 933 N. Cherry Av, Tucson, AZ 85721
³ On leave at MPIA, Heidelberg, Germany
⁴ Caltech, 1200 E. California Blvd, Pasadena, CA 91125
⁵ Hubble Fellow

TABLE 1
NIR VEGA MAGNITUDES OF J0303-0019

Y	J	H	K_s
20.60 ± 0.14	20.44 ± 0.08	19.78 ± 0.08	18.95 ± 0.09

ground subtraction, rectification and combination of the individual frames in one observing block. We used sky lines to determine the wavelength calibration, obtaining an absolute 1σ error of 3 and 7 \AA , respectively, in Y and K band. One-dimensional spectra were extracted from the pipeline products in IRAF. B and G stars with known NIR photometry were used to correct for telluric absorption and initial flux calibration of the one-dimensional spectra. Finally, the one-dimensional spectra were averaged to obtain the final spectra. These were flux calibrated using the broad band magnitudes obtained with the Calar Alto 3.5m telescope (see Sec. 2.2). The reduction is similar to that carried out by K07, where more details are reported.

2.2. Near-infrared broad band imaging

For accurate flux calibration, the QSO SDSS J0303-0019 was imaged with the prime-focus NIR camera Omega2000 (Kovács et al. 2004) at the 3.5m telescope at Calar Alto, Spain. This instrument has a $2k \times 2k$ HAWAII-2 detector with a pixel scale of $0.45''$, resulting in a field of view of $15.4' \times 15.4'$. J0303-0019 was observed on September 10 and 11, 2008, for 20, 20, 25, and 77 minutes in Y , J , H , and K_s bands, respectively. After dark subtraction and flat fielding with twilight exposures, the images were sky subtracted, registered and averaged with XDIMSUM⁶ in IRAF⁷. The seeing full width at half maximum (FWHM) on the combined images is $1.3''$, $1.4''$, $1.3''$, and $1.0''$, respectively. The combined images were astrometrized using the public service provided by *astrometry.net* (Hogg et al. 2008) using a second order polynomial to correct for distortions (which are small for Omega2000). Subsequently, we used about 80 stars from the 2MASS All-Sky Catalog of Point Sources (Skrutskie et al. 2006) to obtain the magnitude zero points. For Y -band, we used the UKIDSS second data release (Warren et al. 2007) catalog. Only half of the observed field is covered by UKIDSS, but this still provides 31 stars usable for the flux calibration. Systematic errors in the flux calibration are estimated to be below 0.1 mag. The resulting fluxes (using MAG_BEST in SExtractor, Bertin & Arnouts 1996) are reported in Table 1.

3. RESULTS

3.1. Optical and NIR spectra

In the top panel of Fig. 1, we show a close-up version of the optical spectrum, first presented in Jiang et al. (2008), taken at the W.M. Keck Observatory. For comparison, the SDSS QSO composite spectrum published by Vanden Berk et al. (2001, dashed curve), normalized to emission line free regions of our observed spectra, is overlaid, showing that the emission lines of J0303-0019 are much stronger and narrower than those present in the

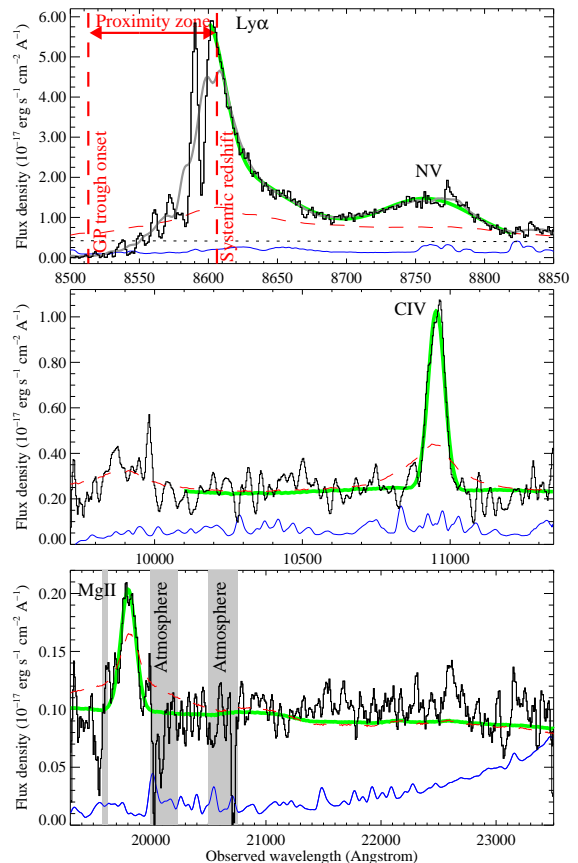


FIG. 1.— *Top*: Optical spectrum of J0303-0019 (black histogram), the same spectrum smoothed over 20 \AA (thick grey curve) and the noise per pixel (blue line). A simultaneous fit (thick green curve) of the N V line and the broad and narrow components of the Ly α line is over plotted on top of a power-law with slope of $\alpha_\lambda = -1.5$, normalized to a line free region of the spectrum (short-dashed line). In addition, the wavelength of the onset of the GP trough and of Ly α at the systemic redshift are indicated by vertical dashed lines. The normalized SDSS QSO composite spectrum by Vanden Berk et al. (2001) is over plotted in red for a visual comparison of the line widths. *Middle and bottom*: NIR Y and K band spectra of J0303-0019, including the C IV and Mg II lines, respectively, smoothed over 5 pixels. The grey regions are seriously affected by sky lines and omitted from the fit. Lines and colors as in top panel. The slope of the power-law continuum here is $\alpha_\lambda = -1.0$.

composite spectrum. We have made a simultaneous fit of the broad and narrow Ly α and N V lines in the optical spectrum, after subtracting a standard (Vanden Berk et al. 2001) power law continuum with a slope $F_\lambda \propto \lambda^{-1.5}$ as in Jiang et al. (2008). We fit only the spectrum redwards of the strong absorption feature seen in the Ly α line. The best fit parameters are listed in Table 2, and the best fit curves are over plotted in Fig. 1. The equivalent width (EW) and FWHM of N V measured by us are about 20% higher than those reported by Jiang et al. (2006), who fixed the central wavelength of all fitted lines to the same redshift.

In the middle and bottom panels of Fig. 1, we show the VLT ISAAC Y - and K -band spectra, containing the C IV and Mg II emission lines, respectively. There is also a tentative detection of Si IV/O IV]1398 at 9900 \AA in the Y -band, which we do not try to fit. The obtained NIR photometry of J0303-0019 (Table 1) is consistent with a power law SED with slope $\alpha_\lambda = -1.5$, as measured in

⁶ XDIMSUM is a variant of the DIMSUM package developed by P. Eisenhardt, M. Dickinson, S.A. Stanford, and J. Ward.

⁷ IRAF is distributed by NOAO, which are operated by AURA, Inc., under cooperative agreement with NSF.

TABLE 2
J0303-0019 EMISSION LINE MEASUREMENTS

Line	α	z	λ_{central} Å	FWHM ^a Å	FWHM ^a km s ⁻¹	Flux ^b 10 ⁻¹⁷ ergs	EW ₀ Å	M _{BH} 10 ⁸ M _⊙	r _{Edd} ^c
Ly α (broad)	-1.5	6.073 \pm 0.001	8599 \pm 1	125 \pm 5	4350 \pm 165	255 \pm 6	87 \pm 2		
Ly α (narrow) ^d				29 \pm 2	1000 \pm 70	109 \pm 11	37 \pm 4		
N V		6.063 \pm 0.001	8758 \pm 1	81 \pm 2	2760 \pm 80	90 \pm 2	32 \pm 1		
C IV	-1.5	6.071 \pm 0.001	10953 \pm 1	65 \pm 2	1780 \pm 65	54 \pm 2	37 \pm 1	1.7 \pm 0.1	1.8 \pm 0.2
C IV	-1.0	6.071 \pm 0.001	10953 \pm 1	65 \pm 3	1772 \pm 70	54 \pm 2	36 \pm 1	1.6 \pm 0.1	1.9 \pm 0.2
C IV	0.0	6.071 \pm 0.001	10953 \pm 1	64 \pm 3	1760 \pm 70	53 \pm 2	35 \pm 1	1.5 \pm 0.1	2.0 \pm 0.2
Mg II	-1.5	6.078 \pm 0.001	19804 \pm 4	149 \pm 9	2261 \pm 130	16 \pm 1	25 \pm 1	2.3 \pm 0.3	1.3 \pm 0.2
Mg II	-1.0	6.078 \pm 0.001	19803 \pm 4	154 \pm 8	2340 \pm 125	17 \pm 1	27 \pm 1	2.5 \pm 0.3	1.2 \pm 0.1
Mg II	0.0	6.077 \pm 0.001	19801 \pm 3	167 \pm 8	2525 \pm 120	19 \pm 1	32 \pm 1	3.0 \pm 0.3	1.0 \pm 0.1

^aFull width at half maximum in Å (observed frame) and km s⁻¹ (rest frame)

^bFlux in 10⁻¹⁷ erg cm⁻² s⁻¹

^cEddington ratio: L_{bol} / L_{Edd} (CIV or MgII)

^dCentral wavelength fixed to that of the broad Ly α line

lower redshift QSOs (Vanden Berk et al. 2001). Imperfect flux calibration of the NIR spectra, however, may affect the slope of the reduced Y and K band spectra. Indeed, the slope observed in the K band seems redder and may be fit better by a slope of $\alpha_\lambda = -1.0$ or even $\alpha_\lambda = 0$. As the NIR spectra are too short and the data not of sufficient quality to constrain the slope, we carry out emission line fits employing a range of slopes α_λ fixed to $= 0, -1.0$, and -1.5 , to cover the complete range of plausible slopes. We take the slope of $\alpha_\lambda = -1.0$ as the best compromise and use the parameters derived from fits employing the two extreme values to construct conservative error estimates on the fitted parameters. The C IV and Mg II lines are fit by single Gaussian functions on top of the co-addition of the power-law continuum, a Balmer pseudo-continuum and a template of Fe II lines (see also Kurk et al. 2007). The strength of the latter two components were scaled with the power-law continuum, according to their proportions in the composite QSO spectrum by Vanden Berk et al. (2001). As the strength of the Fe II emission is not well constrained by the current spectra, but clearly lower than four times the strength in the SDSS composite spectrum, we have also carried out the fitting assuming a four times stronger and four times weaker Fe II contribution to establish proper error estimates.

The resulting best-fit parameters are displayed in Table 2. The C IV and Mg II lines have (rest frame) FWHM₀ less than 2000 and 2600 km s⁻¹, and EW₀ of 36 \pm 1 Å and 27 $^{+5}_{-2}$ Å, respectively. The mean FWHM₀ of these lines in the SDSS QSO sample of Shen et al. (2008, hereafter S08) is 5700 and 5850 km s⁻¹, respectively. Only 2% and 1% of the SDSS QSOs have C IV and Mg II FWHM₀ smaller than 2000 and 2600 km s⁻¹, respectively.

3.2. Black hole mass measurements

The widths of the Mg II and C IV lines, combined with an independent estimate of their characteristic distance from the center, can be used as a measure of the mass of the black hole (M_{BH}). The relation between line width, luminosity and M_{BH} has been calibrated empirically at low redshift using reverberation mapping (e.g., Kaspi et al. 2000). As in K07 and Jiang et al. (2007), we use the relations for C IV and Mg II presented by Vestergaard & Peterson (2006) and McLure & Dunlop (2004),

respectively, which are also those applied to a sample of more than 60,000 SDSS QSOs by S08. Due to the scatter of individual data points around this relation M_{BH} can be determined only within a factor of three. For J0303-0019, we derive M_{BH} with these methods and take into account the range of power-law slopes and Fe II template strength described in Sec. 3.1. We obtain M_{BH} of 1.6 $^{+0.1}_{-0.3}$ and 2.5 $^{+0.5}_{-0.4}$ × 10⁸ M_⊙, respectively, from the C IV and Mg II lines. These are the lowest M_{BH} derived in a $z > 6$ QSO to date, showing that, with this sample of fainter $z \sim 6$ QSOs, we are indeed probing down the mass function of BHs. We note that the central wavelength of the C IV line is blue shifted by 350 km s⁻¹ w.r.t. the Mg II line. According to S08, this modest shift (≤ 1000 km s⁻¹) implies that the C IV line profile is dominated by gravitational effects and that M_{BH} can therefore be reliably estimated from this line.

The M_{BH} derived from the line widths and corresponding Eddington luminosities of log L_{Edd} = 46.31 $^{+0.02}_{-0.09}$, and 46.51 $^{+0.08}_{-0.07}$ ergs⁻¹, respectively, are small compared to the QSO's bolometric luminosity of log L_{bol} = 46.59 \pm 0.04 ergs⁻¹, implying a high Eddington ratio (r_{Edd}). From optical, IR, and radio data (L. Jiang et al, in prep.), the bolometric luminosity of J0303-0019 is determined as in Jiang et al. (2006) to be log L_{bol} = 46.59 ergs⁻¹. It is close to the values of log L_{bol} = 46.62, and 46.65 ergs⁻¹ obtained using the monochromatic luminosities at 1350 Å and 3000 Å, respectively, and the bolometric correction factors⁸ employed by S08 (BC₁₃₅₀ = 3.81, BC₃₀₀₀ = 5.15). Reconciling these values, we obtain the estimated bolometric luminosity stated above. The Eddington ratio of most QSOs is between 0.01 and 1 and only 804 out of the 62,185 SDSS with M_{BH} determined from their line-width have r_{Edd} > 1 (S08). The Eddington ratios for J0303-0019 derived from the C IV and Mg II lines are r_{Edd} = 1.9 $^{+0.2}_{-0.4}$ and 1.2 $^{+0.3}_{-0.2}$ (see Table 2 and Fig. 2). Less than 2% and 0.2% of the SDSS QSOs have such an r_{Edd}(C IV) > 1.9 and r_{Edd}(Mg II) > 1.2. Even if we assume that the other four (faint) $z \sim 6$ QSOs of the complete sample of QSOs discovered in the SDSS Deep Stripe (Jiang et al. 2008) have r_{Edd} < 1.2, the fraction of L_{bol} < 10⁴⁷ ergs⁻¹ QSOs at $z \sim 6$ with r_{Edd} > 1.2

⁸ These bolometric correction factors are multiplicative in flux, unlike the common definition in units of magnitude.

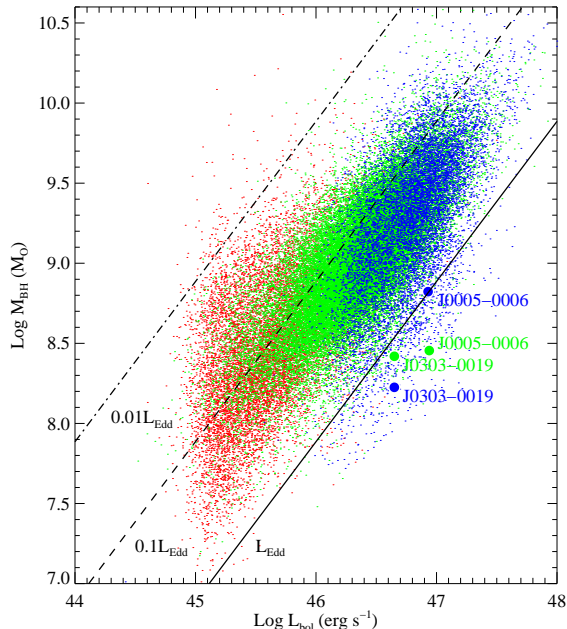


FIG. 2.— The accretion luminosity of J0303-0019 and J0005-0006: the figure shows the $M_{\text{BH}} - L_{\text{bol}}$ diagram reproduced from S08, including $\sim 60,000$ SDSS QSOs at $0.1 \leq z \leq 4.5$. Colors show M_{BH} estimates using the following virial estimators: red for $H\beta$, green for Mg II, blue for C IV. Three diagonal lines show 0.01, 0.1, and 1 L_{Edd} , as indicated. Superposed are the data points for J0303-0019 (this work) and for J0005-0006 (K07). Here, we have applied the cosmology specified in S08, resulting in M_{BH} (L_{bol}) larger by 5% (7%), but r_{Edd} similar to those in our cosmology.

is 33%, almost 40 times higher than at lower redshifts.

3.3. Abundance indicators

The chemical composition of gas clouds in the BLR can be explored by comparing observed emission line ratios to models. The heavy elements in the BLR are products of the star formation history in the host galaxy and therefore indicators of past star formation in at least the very center of the host. Nagao et al. (2006) present several emission line ratios observed in SDSS QSOs at $2.0 \geq z \geq 4.5$ and models explaining the ratios. According to Nagao et al., the strength of the N V/C IV ratio is strongly correlated with the luminosity of the QSO, which can be interpreted in terms of higher gas metallicity in more luminous QSOs. Although J0303-0019 is one of the faintest QSOs at $z \sim 6$, it has a M_B of -26.2 , which makes it moderately luminous in comparison with the SDSS QSOs studied by Nagao et al.. We measure a ratio of $N\text{ V}/\text{C IV} = 1.61 \pm 0.07$, the highest ratio among the known $z \sim 6$ QSOs, and also higher than those measured in the composite spectra of quasars in the luminosity range $-25.5 > M_B > -26.5$ by Nagao et al. (2006). This suggests that the BLR has a high metal abundance, possibly as high as $10Z_{\odot}$ (see Fig. 29 in Nagao et al. 2006), but the authors warn that estimates of the BLR metallicity using only emission line ratios involving N V might be quite uncertain (see also Hamann et al. 2002).

3.4. Strömgren sphere

The intense UV radiation of the QSO keeps a region around the QSO ionized, the Strömgren sphere, which will actually only be spherical if the IGM surrounding

the QSO is homogeneous. Outside this region, UV photons are absorbed by neutral hydrogen and this causes complete absorption blueward of the wavelength of redshifted Ly α , the so-called GP trough (Gunn & Peterson 1965). For reasons discussed in Fan et al. (2006b), the Strömgren sphere radius is difficult to measure and we rather use the size of the proximity zone (R_P), defined as the region in which the transmitted flux is $>10\%$ of the (extrapolated) continuum emission when smoothed to a resolution of 20 \AA (as shown by the grey line in Fig. 1). We measure the blue edge of this region to be at $8513 \pm 1 \text{ \AA}$ (dashed line in Fig. 1). Combined with the systemic redshift of $z = 6.078$ derived from the Mg II line (redmost dashed line in Fig. 1), we compute (K07) the co-moving radius of the Strömgren sphere to be $R_S = 4.5 \pm 0.3 \text{ Mpc}$. This is a typical value for luminous $z \sim 6$ QSOs (see, e.g., K07, Walter et al. 2003; Fan et al. 2006a). The average size of QSO Strömgren spheres, however, decreases by a factor ~ 2.5 over $5.7 < z < 6.4$, consistent with an increase of the neutral fraction with redshift (Fan et al. 2006b).

4. DISCUSSION AND CONCLUSION

SDSS J0303-0019 has the lowest BH mass known at $z \sim 6$ and is a truly peculiar QSO: it has one of the highest Eddington ratios observed for a QSO, it has the highest N V/C IV ratio observed in $z \sim 6$ QSOs, which is also significantly higher than that observed in lower redshift composite spectra of QSOs, and it is one of the two $z \sim 6$ QSOs that is not detected in deep $24 \mu\text{m}$ observations (Jiang et al. 2006, L. Jiang et al. in prep.). The other QSO which is not detected at $24 \mu\text{m}$ is SDSS J000552.34-000655.8 (hereafter J0005-0006), which also has a high Eddington ratio: 2.4 as derived from the Mg II based M_{BH} and 1.0 as derived from the C IV based M_{BH} (K07). Detections at 250 GHz and 1.4 GHz have also been attempted but neither of the objects were detected down to rms values of 0.51, 0.48 mJy and 62, 130 μJy , respectively (Wang et al. 2008). In contrast, these QSOs were detected at 3.6, 4.5 and $5.8 \mu\text{m}$ with IRAC/Spitzer (Jiang et al. 2006, L. Jiang et al. in prep.), implying a rest frame $3.5 \mu\text{m}/4400 \text{ \AA}$ ratio far lower than for any object in the $z \sim 6$ QSO sample, and lower than for any of the PG QSOs observed by Neugebauer et al. (1987) and Haas et al. (2000, 2003) for which the sensitivity at $3.5 \mu\text{m}$ rest-frame is not an issue. Jiang et al. (2006) show that the optical/IR SEDs of the observed $z \sim 6$ QSOs can be fit by two components: a power-law representing an accretion disk and a black-body representing hot dust. The respective (1σ) upper limits of 21 μJy and 9 μJy at $24 \mu\text{m}$ for J0303-0019 and J0005-0006, significantly lower than the expected flux of $\sim 160 \mu\text{Jy}$ based on SEDs of other $z \sim 6$ QSOs, suggests the absence of hot dust. The implied lack of dust could be explained if the gas is metal-poor, as in a galaxy host which has not experienced major star formation yet. However, this interpretation would contradict the potentially high metallicity based on the measured N V/C IV ratio. Alternatively, the non-detection of the hot dust component could be due to different dust properties, or due to a surrounding cool dust torus hiding the hot component (Jiang et al. 2006).

We conclude that, with the observation of QSOs with bolometric luminosity $\lesssim 10^{47} \text{ erg s}^{-1}$, we start to probe a

population of QSOs that shows different observed properties as compared to higher luminosity $z \sim 6$ QSOs and lower-redshift QSOs of all luminosities. We can only speculate that the hosts of the lower-luminosity QSOs at $z \sim 6$ may be younger than higher-luminosity QSOs at the same redshift because the host galaxies of the latter are more massive and have therefore formed earlier. It is, however, unclear at this stage what physical mechanisms are causing the observed differences.

We thank the anonymous referee for comments that helped to improve the paper. Based on observations carried out at the European Southern Observatory, Chile (Program No. 080.A-0794) and at the Calar Alto Observatory, Spain. JK acknowledges financial support from *Deutsche Forschungsgemeinschaft* (DFG) grant

SFB 439. XF and LJ acknowledge supports from NSF grants AST 03-07384 and AST 08-06861 and a Packard Fellowship for Science and Engineering. XF acknowledges additional support from the Max Planck Society and a Guggenheim Fellowship. DR acknowledges support from NASA through Hubble Fellowship grant HST-HF-01212.01A awarded by the STScI, operated by AURA, under contract NAS 5-26555. This publication makes use of data products from the Two Micron All Sky Survey, which is a joint project of the University of Massachusetts and the Infrared Processing and Analysis Center/California Institute of Technology, funded by the National Aeronautics and Space Administration and the National Science Foundation.

Facilities: VLT:Antu, CAO:3.5m ()

REFERENCES

- Barth, A. J., et al. 2003, *ApJ*, 594, L95
 Bertin, E., & Arnouts, S. 1996, *A&AS*, 117, 393
 Fan, X., et al. 2006a, *ARA&A*, 44, 415
 —. 2006b, *AJ*, 132, 117
 Freudling, W., et al. 2003, *ApJ*, 587, L67
 Gunn, J. E., & Peterson, B. A. 1965, *ApJ*, 142, 1633
 Haas, M., et al. 2003, *A&A*, 402, 87
 —. 2000, *A&A*, 354, 453
 Hamann, F., et al. 2002, *ApJ*, 564, 592
 Hogg, D. W., et al. 2008, in *ASP Conference Series*, Vol. 394, ADAS XVII, ed. R. W. Argyle, P. S. Bunclark, & J. R. Lewis, 27
 Iwamuro, F., et al. 2004, *ApJ*, 614, 69
 Jiang, L., et al. 2008, *AJ*, 135, 1057
 —. 2006, *AJ*, 132, 2127
 —. 2007, *AJ*, 134, 1150
 Kaspi, S., et al. 2000, *ApJ*, 533, 631
 Kovács, Z., et al. 2004, in *SPIE Conference Series*, ed. J. D. Garnett & J. W. Beletic, Vol. 5499, 432
 Kurk, J. D., et al. 2007, *ApJ*, 669, 32
 Maiolino, R., et al. 2003, *ApJ*, 596, L155
 McLure, R. J., & Dunlop, J. S. 2004, *MNRAS*, 352, 1390
 Moorwood, A., et al. 1998, *The Messenger*, 94, 7
 Nagao, T., et al. 2006, *A&A*, 447, 157
 Neugebauer, G., et al. 1987, *ApJS*, 63, 615
 Pentericci, L., et al. 2002, *AJ*, 123, 2151
 Shen, Y., et al. 2008, *ApJ*, 680, 169
 Skrutskie, M. F., et al. 2006, *AJ*, 131, 1163
 Vanden Berk, D. E., et al. 2001, *AJ*, 122, 549
 Vestergaard, M., & Peterson, B. M. 2006, *ApJ*, 641, 689
 Walter, F., et al. 2003, *Nature*, 424, 406
 Wang, R., et al. 2008, *ApJ*, 687, 848
 Warren, S. J., et al. 2007, *ArXiv Astrophysics e-prints*
 Willott, C. J., et al. 2003, *ApJ*, 587, L15